

Phase domain walls in coherently driven Bose-Einstein condensates

S. S. Gavrilov

Institute of Solid State Physics RAS, 142432 Chernogolovka, Russia

(Dated: August 5, 2025)

We consider coherent states of weakly interacting bosons under the conditions of external resonant excitation, with a focus on a two-dimensional polariton fluid driven by a plane electromagnetic wave near the ground state. The coherent driving breaks the $U(1)$ symmetry explicitly, which prevents the occurrence of quantum vortices in a uniform scalar condensate. Surprisingly, a spinor (two-component) system of the same kind admits topological excitations, such as domain walls of relative phase or confined half-vortex molecules, typical of a freely evolving spinor Bose system. Opposite-phase domains arise from the spontaneous breakdown of the spin symmetry (\mathbb{Z}_2). Domain walls form with time even when the initial state of the system is uniform or completely disordered; they fall into different topological types distinguished by the total phase variation in the transverse direction.

I. INTRODUCTION

A coupled pair of spatially overlapping Bose-Einstein condensates (BECs) has complex topological excitations that cannot be reduced to the case of one scalar BEC. Typical examples of such systems include atomic BECs with coexistent hyperfine species [1] and two-band superconductors [2]. In one dimension, they admit the sine-Gordon kinks characterized by the 2π jump of the relative phase of order parameters [3, 4]; in two dimensions, the kink turns into a domain wall which gives birth to more complicated objects such as bound states of half-quantized vortices (HQVs) [5, 6]. The mechanism of the HQV pairing on a domain wall was found to be formally similar to quark confinement [7, 8]. The underlying mean-field theory attracts much interest owing to its broad scope and very rich physics it contains in spite of conceptual simplicity [9].

In this work, we investigate a dissipative BEC coupled to an external classical field whose frequency is close to the BEC ground-state level. Such a system is found to admit stable domain walls and HQV molecules which arise spontaneously even when the initial conditions are uniform or, conversely, disordered. The uniform BEC undergoes a spontaneous \mathbb{Z}_2 symmetry breaking that proceeds *nonglobally*, by way of the Kibble-Zurek mechanism [10–12], as soon as the driving field reaches a critical amplitude; in turn, a disordered system exhibits self-organization. Once dynamic equilibrium has established, a number of HQV molecules and domain walls act as elements of complex, inhomogeneous yet internally ordered states whose spatial extent is far beyond any conventional characteristic scale of a BEC.

The minimum model containing the phenomena under consideration is represented by the mean-field equations

$$i\hbar \frac{\partial \psi_{\pm}}{\partial t} = -i\gamma \psi_{\pm} + \frac{\delta H}{\delta \psi_{\pm}^*} \quad (1)$$

for a pair of complex-valued amplitudes $\psi_{\pm} = \psi_{\pm}(\mathbf{r}, t)$, where γ is the decay rate and

$$\begin{aligned} H[\psi_+, \psi_-] = & \int \left[-D(|\psi_+|^2 + |\psi_-|^2) + \frac{\hbar^2}{2m} (|\nabla \psi_+|^2 + |\nabla \psi_-|^2) \right. \\ & + \frac{V}{2} (|\psi_+|^4 + |\psi_-|^4) + \frac{\Omega}{2} (\psi_+^* \psi_- + \psi_-^* \psi_+) \\ & \left. + f(\psi_+ + \psi_- + \psi_+^* + \psi_-^*) \right] d^2 \mathbf{r} \quad (2) \end{aligned}$$

is the energy of a bosonic fluid characterized by mass m , nonlinear interaction strength V , and spin coupling rate Ω . The external field has amplitude f that is assumed to be real-valued and constant; thus, D equals the detuning between the excitation energy level (taken as zero) and BEC ground state ($-D$). In what follows, we suppose that $V > 0$ and $D > \gamma$ and that feasible values of $V|\psi_{\pm}|^2$ can be as great as D .

This theory applies to a cavity-polariton system driven by a resonant light wave [13, 14]. Cavity polaritons are bosonic particles, mixed states of excitons and photons formed in a planar quantum well inside a microcavity. They reach macroscopic coherence either through Bose-Einstein condensation of excitons [15] or, thanks to the photonic part, under coherent optical driving [16]. Two pseudospin states of excitons match the right- and left-handed circular polarizations of light, which gives two polariton components. The polariton-polariton interaction ($\propto V$) comes from the exchange Coulomb interaction of electrons or holes [17, 18]; an inter-component scattering of this kind is usually inhibited [19] and disregarded in (2). At the same time, the two components can be linearly coupled ($\propto \Omega$) owing to the structural anisotropy of a microcavity [20]. The decay rate γ depends on the cavity quality factor.

Apparently, the coherent driving alters the nature of a BEC. The model has the explicitly broken phase symmetry, i. e., it is not invariant under the transformation $\psi_{\pm} \mapsto \psi_{\pm} e^{i\chi}$ (χ being a real number) unless $f = 0$. It might seem unclear if this model ever admits vortices or dark solitons. In fact, they are absent in a scalar (spinless) system driven by a continuous wave with zero in-plane momentum, because the local phase of ψ is fixed by the driving field [21]. The spinor model was found to admit both solitons and vortices, but their relation to the ones typical of the freely evolving BECs remained obscure [22]. Here, we show that a nontrivial crossover exists between the driven and free systems where they get close to each other in the sense of their vacuum states as well as the elementary and topological excitations.

Our general predictions are the most easily understood in the limit $\gamma \ll D \sim \Omega$. Owing to the symmetry breaking, in a wide range of f the system has only two equally feasible vacuum states $\psi_{\pm(\mp)} = \psi_{\mp(\pm)}^* = \sqrt{n} e^{\pm i\alpha}$, where n is constant and α grows from $\pi/2$ to π with increasing f . These solutions differ in the sign of the relative phase $\arg(\psi_+ \psi_-^*) = \pm 2\alpha$ and can be interfaced by a domain wall. The individual phases of ψ_{\pm} inside both domains are determined modulo 2π , so the domain

walls fall into distinct topological types. For instance, when ψ_+ or ψ_- gets switched from $\psi \sim e^{i\alpha}$ to $e^{-i\alpha}$, the respective phase $\phi = \alpha$ can either monotonically decrease down to $-\alpha$ or increase up to $2\pi - \alpha$; thus, it varies by $-\alpha$ or $2\pi - 2\alpha$, whereas the other spin component has to change its phase by 2α or $2\alpha - 2\pi$. As a result, the amount q of the total continuous variation of $(\phi_+ + \phi_-)/2\pi$ across a domain wall takes discrete values $-1, 0, 1$. Dynamical instability of domain walls with $q = 0$ involves spontaneous formation of confined HQV pairs, in analogy to atomic BECs [23–25]. Second, a uniform motion of the $q = 0$ domain wall is counterbalanced by a nonzero spin polarization ($\propto n_+ - n_-$) whose sign is fixed by the direction of motion. A similar phenomenon in atomic BECs, referred to as a *magnetic* domain wall or soliton, was also considered recently [26–28].

By contrast, the $q = \pm 1$ domain walls are quite unusual objects with fundamentally broken spatial and spin symmetries. Two phase gradients $\nabla\phi_{\pm}$ now have the same direction that is determined by q irrespective of the actual solitonic velocity. The spin polarizations and energetically favored directions of motion are opposite for the $q = \pm 1$ domain walls which, thus, cannot transform into each other. At the same time, they can be linked together by a HQV pair and make up a joint, possibly motionless domain wall with alternating $q = \pm 1$ segments. In fact, the steady states which a randomly prepared system approaches with time take the form of such piecewise domain walls containing HQVs. Ordered yet nonstationary states are also possible. For instance, two curvilinear $q = \pm 1$ segments can form a closed contour encapsulating a spot of one domain inside the other which runs as a composite soliton. Alternatively, two half-open domain walls rotate around a HQV pair and so produce rotation of domains in a fixed environment. All such phenomena imply that the $q = \pm 1$ domain walls balance each other dynamically on a large scale.

The paper is organized as follows. In Sec. II, we discuss the very possibility of a free evolution of coherently driven BECs. Section III describes the vacuum states. Having them defined, in Sec. IV, we formulate a boundary-value problem for domain walls and analyze its solutions in the one-dimensional case. Section V deals with domain walls and HQV molecules in two dimensions, paying special attention to long-range collective states (VA) and spontaneous phenomena (VB). Section VI contains concluding remarks. In Appendix A, we specifically consider the system of cavity polaritons and its parameters. Appendix B contains the exact solution to the problem of the vacuum states and respective elementary excitations. The work also has four Supplemental Materials with video presentations of dynamics in some noteworthy cases.

II. SYMMETRY CONSIDERATIONS

In this introductory section, we briefly explain why a driven BEC can behave “like a freely evolving system”. That is a bit arguable; one might suggest that, conversely, the driving field governs both components of the spinor order parameter, in analogy to a damped oscillator driven by a harmonic force, which prevents formation of vortices. It turns out, however,

that such a forced evolution is not absolutely necessary.

Substituting $\psi_{\pm} = \sqrt{n_{\pm}}e^{i\phi_{\pm}}$ in (1) leads one ([29]) to the following continuity equation,

$$\frac{\partial}{\partial t}(n_+ + n_-) = -\nabla(\mathbf{j}_+ + \mathbf{j}_-) - \frac{2\gamma}{\hbar}(n_+ + n_-) - \frac{2f}{\hbar}(\sqrt{n_+}\sin\phi_+ + \sqrt{n_-}\sin\phi_-), \quad (3)$$

where \mathbf{j}_{\pm} are currents, defined as

$$\mathbf{j}_{\pm} = -\frac{i\hbar}{2m}(\psi_{\pm}^*\nabla\psi_{\pm} - \psi_{\pm}\nabla\psi_{\pm}^*) = \frac{n_{\pm}\hbar}{m}\nabla\phi_{\pm}. \quad (4)$$

The last term in (3) represents the source of excitation. In the case of a one-component system (i. e., when one of ψ_{\pm} is zero or ψ_+ and ψ_- are identical), this driving term invalidates the conventional steady-state vortex solutions such that $\nabla n \neq 0$ and $\nabla\phi \neq 0$ but $(\nabla n)(\nabla\phi) = n\nabla^2\phi = 0$; moreover, all actual steady states prove to be uniform [30]. On the other hand, the two-component system under certain conditions has a weak symmetry of the form $\psi_+ + \psi_- = \psi_+^* + \psi_-^*$, so that quantity

$$K = -(\sqrt{n_+}\sin\phi_+ + \sqrt{n_-}\sin\phi_-) \quad (5)$$

turns to zero even when both components vary in space. In this case the driving term vanishes from (3) irrespective of f .

The considered weak symmetry $K = 0$ is equivalent to invariance of the density of energy (\mathcal{H}) under the transformation $\psi_{\pm} \mapsto \psi_{\pm}e^{i\chi}$ for small χ . Directly from (2) one can see that $\mathcal{H}(\psi_{\pm}e^{i\chi}) - \mathcal{H}(\psi_{\pm})$ tends to $2\chi f K$ when $\chi \rightarrow 0$. In fact, it is just a special case of Noether’s theorem that invariance under *infinitesimal global phase shift* yields the continuity equation with no external sources (e. g., [31]). Thus, condition $K = 0$ means that not only moduli $\sqrt{n_{\pm}}$ but also phases ϕ_{\pm} of order parameters are partially unlocked. As a result, certain features of freely evolving BECs, such as spontaneously formed HQV molecules and moving domain walls, are no longer forbidden.

An important question is when such a symmetry is obeyed. Since the theory is spin-symmetric, Eqs. (1) always admit trivial uniform solutions with $\psi_+ = \psi_-$ which have fixed phases. They, however, lose stability in some range of f , giving way to a doublet of the true vacuum states with $\psi_+^* = \psi_-$ at $\gamma \rightarrow 0$. The stationary $q = 0$ domain walls as well as HQV molecules represent the nonuniform states with $K = 0$. The symmetry of the $q = \pm 1$ domain walls is reduced further, namely, function $K(\mathbf{r})$ becomes nonzero and antisymmetric across the wall, which manifests broken parity. Nevertheless, all domain walls are capable of a solitonic motion, because the mean value of K is zero.

The above considerations help us to compare our results to the previously known mechanisms of vortex formation in resonantly excited polariton systems. In all cases, the key point is to get rid of the phase locking of the driven fluid with respect to the driving optical field. Previously, this was done by making the system explicitly inhomogeneous in space or time. For instance, vortices can be “injected” immediately by means of short-term excitation pulses with appropriate shapes [32–34]. Alternatively, one can excite the system by a tightly focused Gaussian beam with a nonzero in-plane momentum, so

that pumped polaritons permanently run out of the excitation spot [21, 35–37]. The third mechanism employs the scattering of the pumped mode into a pair of new macroscopically occupied modes that have different frequencies [38–42]. In all such situations (see also [43, 44]), some part of a driven system remains free at a certain time, place, or energy level; as a rule, the vortex positions are predetermined. By contrast, our scenario does not rely upon any inhomogeneity of the model and f is constant; at the same time, vortices and domain walls move freely owing to zero-mean K . However, this is possible only when γ is much smaller than Ω . Relevant parameters of the system of cavity polaritons are discussed in Appendix A.

III. VACUUM STATES

The vacuum states, which are purely one-mode solutions to Eqs. (1), exist for each f , because the nonlinear interaction is defocusing ($V > 0$) and the model is spatially uniform; and since the system is dissipative ($\gamma > 0$), both order parameters ψ_{\pm} can be expected to oscillate at the frequency of the driving field (taken as zero). However, although the model is explicitly spin-symmetric, the one-mode solutions with $\psi_+ = \psi_-$ are unstable a wide range of f .

In Appendix B, we find all vacuum states and elementary excitations in a general form. Here, we only illustrate the main features of the relevant solutions at $D \sim \Omega \gg \gamma$.

The considered vacuum states possess a reduced spin symmetry of the form $\psi_+^* \approx \psi_-$. They exist in the interval of Vf^2 from $Vf_1^2 = 2\gamma\Omega(D + \Omega)$ to $Vf_2^2 = \Omega^2(D + \Omega/2)$ and, moreover, turn out to be the sole kind of stable one-mode solutions if $f_1^2 \leq f^2 \leq 0.3f_2^2$. Densities $n_{\pm} = |\psi_{\pm}|^2$ are almost independent of f and equal to μ/V , where

$$\mu = D + \frac{\Omega}{2}. \quad (6)$$

The phases of spin components in two vacuum states, $\alpha_{\pm(\mp)}$, are nearly equal to $\pm\alpha$, where α varies from about $\pi/2$ to π as $\alpha \approx \arccos(-f/f_2)$, provided that $f > 0$. At $f = f_2$, the solution becomes symmetric and single-valued. Characteristic dependences of $n_+ + n_-$ and $\cos(\alpha_+ - \alpha_-) \approx \cos 2\alpha$ on f^2 are shown in Figs. 1(a) and 1(b).

Bearing in mind optical experiments, it is convenient to express the solutions in terms of the Stokes vector components. Proceeding from unitary transformation $\psi_{\pm} = (\psi_H \mp i\psi_V)/\sqrt{2}$, where $\psi_{H,V}$ are the fields with mutually orthogonal “horizontal” and “vertical” polarizations, one defines

$$S_1 = \frac{|\psi_H|^2 - |\psi_V|^2}{|\psi_H|^2 + |\psi_V|^2}, \quad S_2 = \frac{\psi_H^* \psi_V + \psi_V^* \psi_H}{|\psi_H|^2 + |\psi_V|^2}, \quad (7)$$

which are the degrees of linear polarization in two Cartesian bases rotated relative to each other by $\pi/4$. The third component of the Stokes vector,

$$S_3 = \frac{|\psi_+|^2 - |\psi_-|^2}{|\psi_+|^2 + |\psi_-|^2}, \quad (8)$$

represents the degree of circular polarization. The whole Stokes vector $\mathbf{S} = (S_1, S_2, S_3)$ has the length of unity.

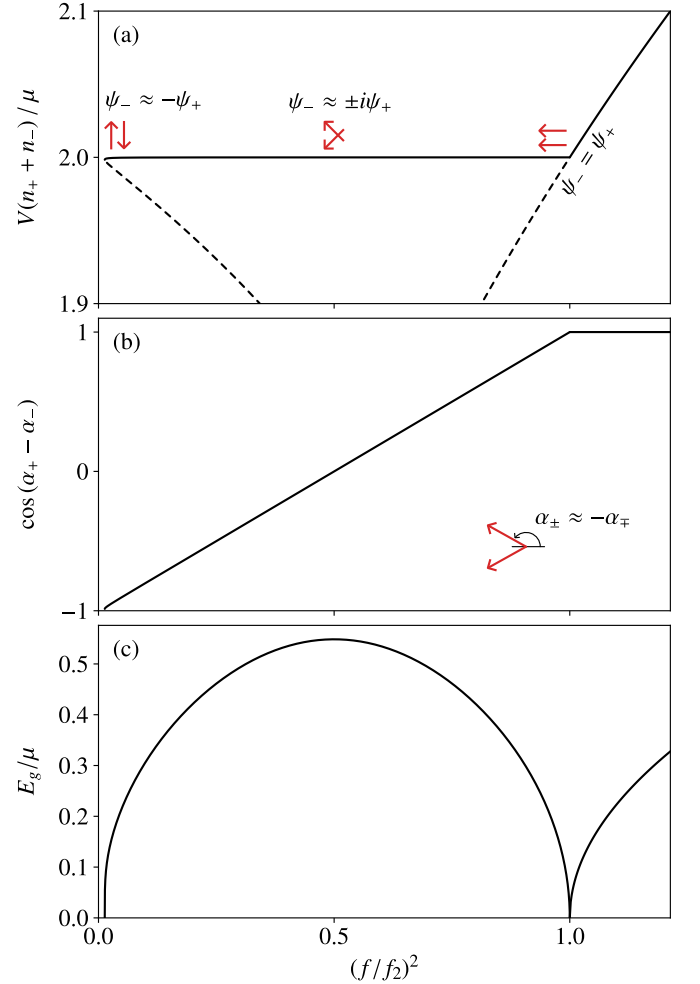


FIG. 1. Vacuum states depending on f^2 . (a) Density of the full number of particles according to (B11) for $f < f_2$ and (B6) for $f \geq f_2$. The dashed curves show unstable solutions. (b) Cosine of the relative phase of ψ_{\pm} according to (B13) (exactly) or (B23) (approximately). The arrows in (a) and (b) indicate individual phases α_{\pm} . (c) Energy gap between the vacuum state and elementary excitations according to (B15) for $f < f_2$ and (B7) for $f \geq f_2$ (exactly) or (B26) for $f < f_2$ (approximately). Parameters: $D = \Omega$, $\gamma/\Omega = 5 \times 10^{-3}$.

Since $n_+ \approx n_-$ and, thus, $S_3 \approx 0$ for $f \in (f_1, f_2)$, the field is polarized almost linearly. Specifically,

$$\begin{pmatrix} \psi_H \\ \psi_V \end{pmatrix} = \sqrt{2\mu} \begin{pmatrix} \cos \alpha \\ \pm \sin \alpha \end{pmatrix}, \quad S_1 = \cos 2\alpha, \quad S_2 = \pm \sin 2\alpha. \quad (9)$$

Thus, α equals the angle between the polarization directions of the driven and driving fields, $\psi_{H,V}$ and $f_{H,V} = (\sqrt{2}f, 0)$. The two states forming the phase doublet at a given f differ in the sign of S_2 that is directly measurable.

The asymptotic stability of the solutions is ensured by the gap between the vacuum state and elementary excitations. Its width E_g as a function of f is shown in Fig. 1(c). When E_g turns to zero at $f = f_{1,2}$, the dispersion law takes the Bogoliubov form (B27). Remarkably, in this case quantity (6) plays the role of an equilibrium chemical potential. Typical spectra of excitations, gapped and gapless, are shown in Fig. 2.

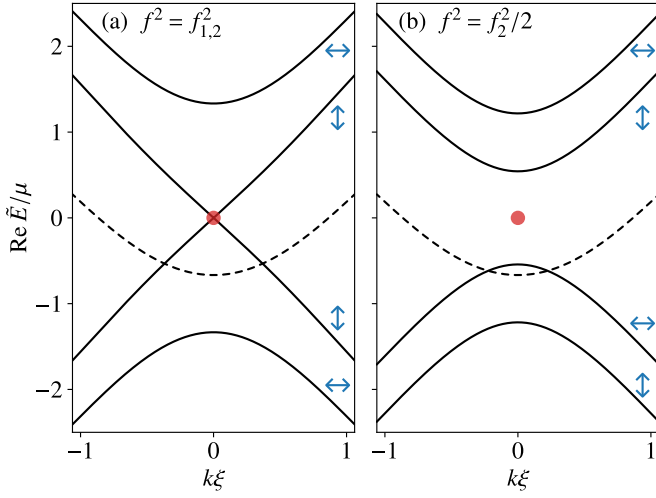


FIG. 2. Spectra of elementary excitations depending on wave number k at $f = f_1$ or $f = f_2$ (a) and $f = \sqrt{2}f_2$ (b) according to (B15) (exactly) or (B25) (approximately). The dashed curve shows the bare dispersion law; the central dot is the driven mode. The gapless spectrum in (a) obeys the Bogoliubov formula (B27). The arrows indicate polarization directions of excitations, horizontal (\leftrightarrow) or vertical (\updownarrow). Parameters as in Fig. 1; $\xi = \hbar/\sqrt{2m\mu}$.

Starting with Figs. 1 and 2, in all illustrations we use a system of “natural” physical units. Specifically, μ represents the densities of the numbers of particles (Vn_{\pm}) and typical shifts of energy levels; the respective healing length $\xi = \hbar/\sqrt{2m\mu}$ is the natural scale and ξ^{-1} is the wave number. The sound velocity in a conventional BEC, $v_s = \sqrt{\mu/m}$, serves as a characteristic velocity.

IV. DOMAIN WALLS IN ONE DIMENSION

Let us find the shape of domain walls in a relatively simple case of the one-dimensional system. Substituting $\psi_{\pm}(x, t) = \psi_{\pm}(x - vt)$ into Eqs. (1) leads one to the following system of time-independent equations in the soliton frame of reference,

$$\frac{\hbar^2}{2m} \frac{d^2 \psi_{\pm}}{dx^2} - i\hbar v \frac{d\psi_{\pm}}{dx} + (D + i\gamma - V\psi_{\pm}^* \psi_{\pm}) \psi_{\pm} - \frac{\Omega}{2} \psi_{\mp} - f = 0. \quad (10)$$

The boundary conditions correspond to the vacuum states and, therefore, should be set rigidly, e. g.,

$$\psi_{-}(-\infty) = \psi_{+}(+\infty) = \sqrt{n_1} e^{i\alpha_1}, \quad (11)$$

$$\psi_{+}(-\infty) = \psi_{-}(+\infty) = \sqrt{n_2} e^{i\alpha_2}, \quad (12)$$

where $n_{1,2}$ and $e^{i\alpha_{1,2}}$ are determined by (B12)–(B14). Below, we take very small γ and assume that $n_1 = n_2$ and $\alpha_1 = -\alpha_2 = \alpha > 0$. Swapping the two domains, i. e., choosing the opposite sign of α or exchanging the right-hand sides in (11) and (12), would result in a physically equivalent situation.

In what follows, we solve this boundary-value problem numerically by means of the fourth order collocation algorithm [45] implemented in SciPy [46]. Technically, to do so

one has to rewrite (10) in the form of eight real-valued equations of the first order.

A. Static domain walls ($v = 0$)

For each given set of parameters and boundary conditions, the above problem can have several topologically different solutions which are distinguished by the total phase variation

$$q = \frac{1}{2\pi} \int_{-\infty}^{+\infty} \left(\frac{d\phi_{+}}{dx} + \frac{d\phi_{-}}{dx} \right) dx. \quad (13)$$

For consistency, swapping the vacuum states in (11) and (12) should be accompanied by the x axis reversal in (13). Typical solutions with $q = 0$ and $q = \pm 1$ obtained at $v = 0$ are represented in Fig. 3.

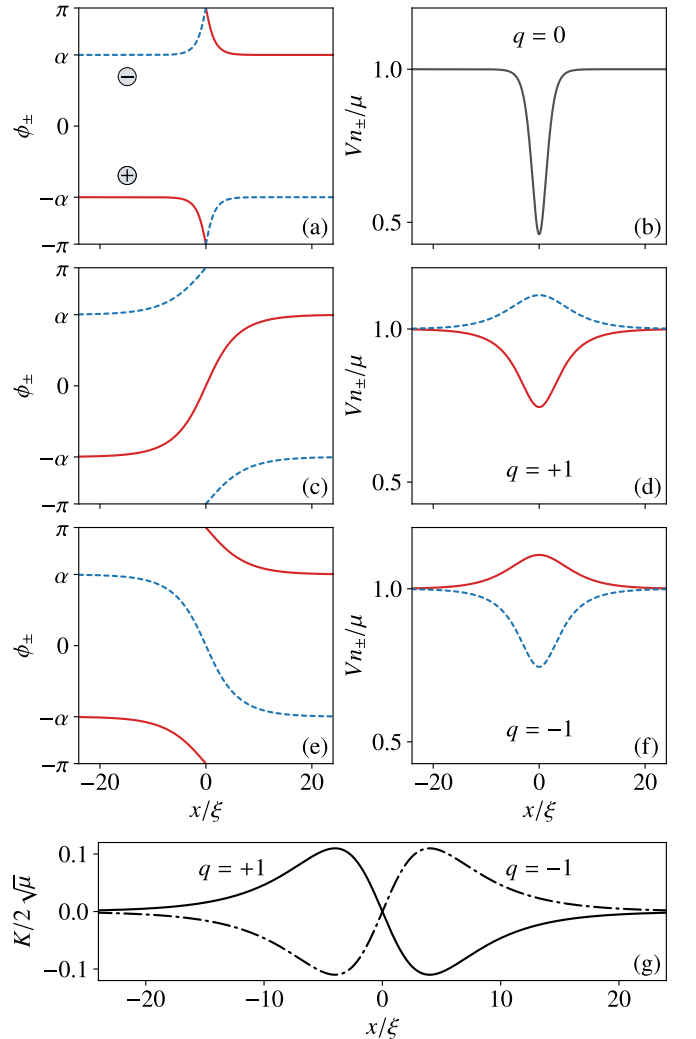


FIG. 3. (a)–(f) Three solutions to boundary-value problem (10)–(12) for $v = 0$ and $f^2/f_2^2 = 0.1$. The left and right sides represent $\phi_{\pm} = \arg \psi_{\pm}$ and $n_{\pm} = |\psi_{\pm}|^2$, respectively; solid and dashed curves correspond to individual components (+ and -). (g) Quantity K (5) across the $q = \pm 1$ domain walls. Parameters: $D = \Omega$, $\gamma/\Omega = 10^{-6}$.

The $q = 0$ domain walls [Figs. 3(a) and 3(b)] retain the symmetry of the form $\psi_+^* = \psi_-$ for each x . Generally, if $\psi_+^* = \psi_-$, phases ϕ_+ and ϕ_- coincide at the center of a domain wall ($x = 0$), being equal to 0 or $\pm\pi$. The solutions with $\phi_{\pm}(0) = 0$ never occurred in our calculations; notice that they would have maximized the last term in (2),

$$\mathcal{H}_f = 2f(\sqrt{n_+} \cos \phi_+ + \sqrt{n_-} \cos \phi_-). \quad (14)$$

In turn, the solutions with $\phi_{\pm}(0) = \pm\pi$ exist in the whole interval (f_1, f_2) .

The $q = \pm 1$ domain walls [Figs. 3(c)–3(f)] have nonzero spin polarizations S_3 and co-directed currents $\mathbf{j}_{\pm} \propto n_{\pm} \nabla \phi_{\pm}$ even at $v = 0$. Moreover, $\nabla(\mathbf{j}_+ + \mathbf{j}_-)$ is also nonzero, which can be attributed only to external driving. To illustrate this point, Fig. 3(g) shows function $K(x)$ that determines the source term in the continuity equation (3). $K(x) > 0$ means that the system has an external source of particles at a given x , compensated by a “negative source” at $-x$. For $q = +1$, the whole picture suggests that particles tunnel from positive to negative x under the external field. In turn, on both sides of $x = 0$ these sources are counterbalanced by the currents with $\nabla(\mathbf{j}_+ + \mathbf{j}_-) \neq 0$, so that Eq. (3) is satisfied statically ($\partial_t n_{\pm} = 0$).

Figure 4 shows how the spatial widths and peak values of n_{\pm} depend on f for different types of domain walls. The widths σ_{\pm} are calculated by fitting the numerically obtained phase patterns $\phi_{\pm}(x)$ with appropriately scaled kinks,

$$\phi(x) = \phi_1 + \frac{2}{\pi}(\phi_2 - \phi_1) \arctan e^{x/\sigma}, \quad (15)$$

where $\phi_{1,2} = \phi(\mp\infty)$. The $q = 0$ and $q = \pm 1$ domain walls are

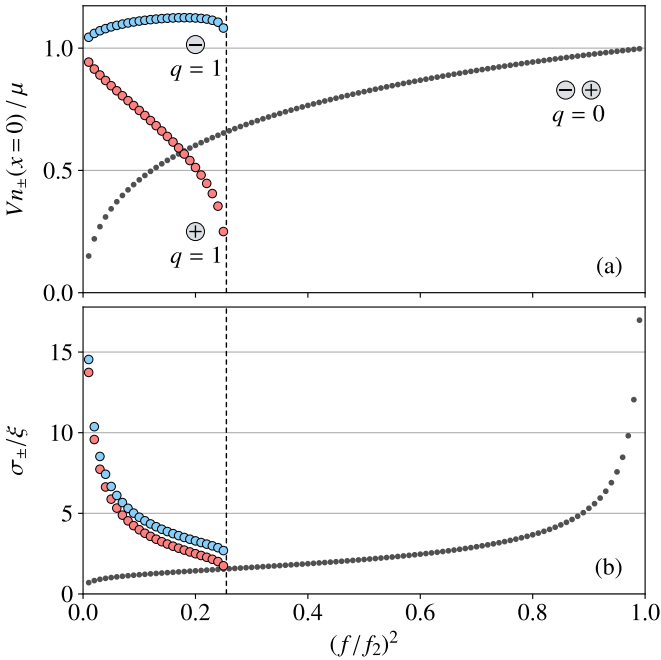


FIG. 4. Peak values of n_{\pm} (a) and spatial widths σ_{\pm} (b) of motionless domain walls depending on f^2 . The dashed vertical line indicates the limiting value of f^2 at which the $q = \pm 1$ domain walls cease to exist. Parameters as in Fig. 3.

seen to behave oppositely. The $q = 0$ solution has the greatest dip in $n(x)$ as well as the minimum σ at $f = f_1$, becomes less pronounced with increasing f , and vanishes at $f = f_2$. Since the states with $\psi_+^* = \psi_-$ are polarized linearly, their features are better understood in terms of the $\psi_{H,V}$ rather than ψ_{\pm} fields. The key point is the phase reversal of ψ_V between the vacuum states [Eq. (9)], owing to which the $q = 0$ domain walls can be seen as dark solitons in ψ_V . With increasing f , they become less pronounced, because the fraction of ψ_V is lowered. The width $\sigma = \hbar / \sqrt{2mE}$ of such domain walls roughly corresponds to energy $E = V\psi_V^2$ in the vacuum states.

In turn, the width of the $q = \pm 1$ domain walls corresponds to their spin imbalance ($E \sim V|n_+ - n_-|$) which grows with f . Notice that the phase jumps of two components across a domain wall, $\pm 2\alpha$ and $\pm 2\pi \mp 2\alpha$, become essentially different at high f and the greater one ($\pm 2\alpha$) is accompanied by a growing dip in $n(x)$. As a result, the spin polarization of the currents remains small ($j_+ \approx j_-$) for each f in spite of increasing $|S_3|$. This branch of solutions is seen to terminate at some point.

B. Motion of domain walls

Let us find out how the characteristics of domain walls depend on their state of motion. In atomic BECs, the energy of a moving soliton typically has a quadratic dependence on its velocity, $H(v) = H(0) + m^*v^2/2$, which allows one to introduce the soliton mass m^* [24, 47]. That mass can be negative, in which case a *dark* soliton gets accelerated upon losing energy through its interaction with thermal excitations.

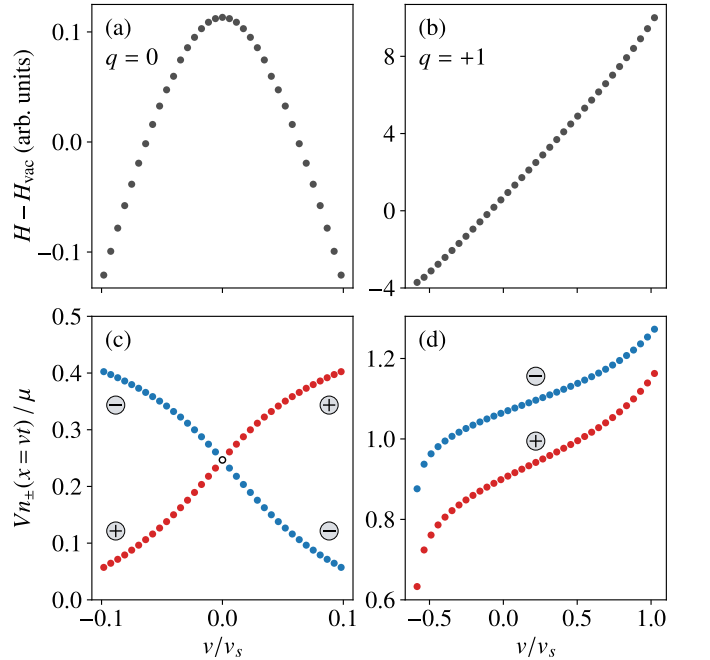


FIG. 5. Energy (2) (a, b) and peak values of n_{\pm} (c, d) as functions of v for the domain walls with $q = 0$ (a, c) and $+1$ (b, d) at $f^2/f_2^2 = 0.025$. Parameters as in Fig. 3; H_{vac} is the vacuum energy; $v_s = \sqrt{\mu/m}$.

Figure 5 shows the dependences of H and peak n_{\pm} on v for the $q = 0$ and $q = 1$ domain walls slightly above the f_1 point. The $q = 0$ state behaves similarly to the 2π magnetic solitons in atomic BECs [26–28]. It has a negative mass and nonzero S_3 whose sign depends on the direction of motion. A pair of the $q = 0$ states with opposite velocities transform into each other continuously. The greatest $|v|$ at which this kind of solutions exists is comparable to $0.1v_s$. As a rule, the sign of the soliton mass is reversed with increasing f .

By contrast, the $q = \pm 1$ domain walls are not characterized by any mass in the usual sense. They have certain signs of S_3 irrespective of v and tend to move in certain preferred directions. The energy is lowered when v and q have opposite signs. Remarkably, both n_+ and n_- decrease upon lowering H , so that a *gray* soliton becomes more *dark* in the course of its spontaneous acceleration. In this respect, our system behaves conversely to the usual BECs in which increasing v acts to smoothen a dark soliton until it reaches the sound velocity and turns into a plane wave. Notice as well that the minimum H in Fig. 5(b) is less than the vacuum energy. Therefore, a domain wall moving with its greatest negative velocity $v \lesssim -0.5v_s$ is expected to be energetically stable.

The above predictions have been verified numerically by solving the dynamical equations (A3) for a two-dimensional polariton system of size $500\xi \times 30\xi$. A video presentation of the solution can be found in Supplemental Material I. In the long dimension (axis x), the boundary conditions were zero owing to high potential walls at both ends, whereas in the short dimension (y) they were periodic. For each y , the initial state along the x axis was the $q = 1$ domain wall obeying Eqs. (10)–(12) at $D = \Omega$, $\gamma/\Omega = 1.5 \times 10^{-4}$, and $f_2/f_2^2 = 0.025$. Finite fluctuations came from the fact that the chosen initial state is not an exact solution for the system in a box. The dynamical equations were solved using the adaptive RK5(4) method by Dormand and Prince [48]. In agreement with our qualitative analysis, it turned out that interaction with fluctuations makes the soliton run in the opposite direction relative to $\nabla\phi_{\pm}$. With time, this soliton becomes “gray” in both spin components, reaches its greatest velocity, and then runs steadily until it hits the end wall. Here, the soliton gets reflected, changes the sign of q , and starts moving back towards the other end wall. Thus, the overall dynamics takes the form of periodic spatiotemporal oscillations of ϕ_{\pm} and S_2 .

Up to now, we supposed that the decay rate γ is extremely small. When it is increased, everything becomes more complicated, in particular, the solutions to Eqs. (1) no longer satisfy the solitonic Eqs. (10). (Technically, the minimized left-hand sides of (10) tend to certain small yet nonzero residual values that increase with γ .) On the other hand, the asymptotic stability of the phase domains *per se* is only enhanced, because all excitations inside them tend to decay on the time scale of \hbar/γ [Eq. (B25)]. As a result, the domain walls survive and still have the $q = \pm 1$ types at small f , however, they become nonstatic even in the soliton frame of reference. The above-considered numerical experiment also displays fast and irregular oscillations of $n_{\pm}(x = vt)$, which suggests that the persistence of the solitonic interface should rather be ascribed to the internally stable domains. In this respect the discussed sys-

tem noticeably differs from the freely evolving atomic BECs in which the (in)stabilities of domains and domain walls mean the same thing.

As a final remark, let us notice that the solutions to Eqs. (10) at $v > 0$ and $\gamma \rightarrow 0$ can also converge to higher-order states with $q \geq 2$. Under normal conditions, such states are unstable in two dimensions, so we do not analyze them in the current work.

V. DOMAIN WALLS IN TWO DIMENSIONS

We have found that the $q = \pm 1$ domain walls tend to move in space. Here, we show that they naturally coexist and balance each other in a two-dimensional system. As a characteristic example, Fig. 6 shows a small piece of a domain wall in the vicinity of its crossover between the $q = \pm 1$ states. Two HQVs are seen to connect them continuously, much as a domain wall itself connects phase domains.

The occurrence of “internally ordered” HQV molecules in a driven BEC agrees with the fact that quantity K (5) is small and smooth even at the singular points. To see this, assume that the n_+ and n_- cores lie on the $y = 0$ axis at $x = 0$ and $x = L > 0$, respectively, and the distribution of ϕ_{\pm} near the cores corresponds to Figs. 6(c) and 6(d), namely,

$$\sin \phi_+ = -\frac{y}{\sqrt{x^2 + y^2}}, \quad \sin \phi_- = \frac{y}{\sqrt{(x-L)^2 + y^2}}. \quad (16)$$

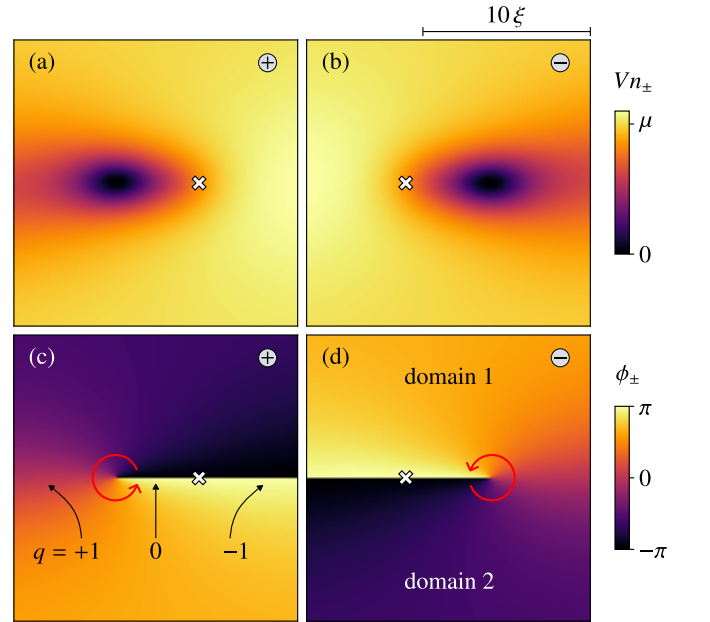


FIG. 6. Characteristic solution having two phase domains, the $q = 0$ and $q = \pm 1$ domain walls, and a HQV molecule. The top and bottom sides show n_{\pm} and ϕ_{\pm} ; the left and right sides correspond to individual spin components (+ and −). The cross marks (x) indicate positions of the opposite-spin vortices. The circular arrows in (c) and (d) indicate the directions in which ϕ_{\pm} vary from $-\pi$ to π . Parameters: $D = \Omega$, $\gamma/\Omega = 5 \times 10^{-3}$, $f^2/f_2^2 \approx 0.13$.

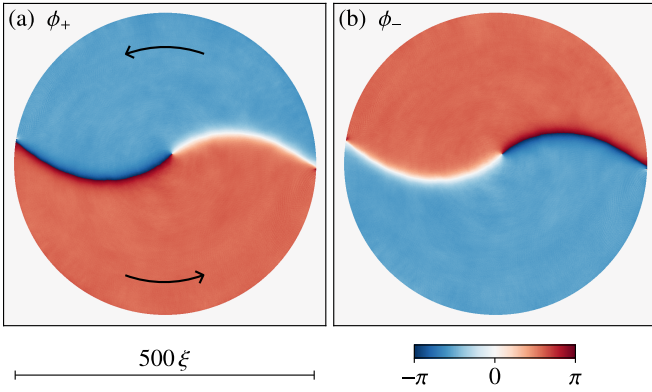


FIG. 7. Persistently rotating solution with symmetric $q = \pm 1$ segments of a domain wall. (a) and (b) represent phases ϕ_{\pm} of two spin components. The arrows indicate the direction of rotation. Parameters: $D = \Omega$, $\gamma/\Omega = 7.5 \times 10^{-4}$, $f^2/f_2^2 = 0.025$. The dynamics is shown in Supplemental Material II.

In the close vicinity of the n_+ core, i. e., at $r = \sqrt{x^2 + y^2} \ll L$, condition $K = 0$ immediately leads to $\sqrt{n_+/n_-} = r/L$. Since n_- behaves regularly, we finally have $\sqrt{n_+} \propto r$ at $r \rightarrow 0$, which corresponds to the shape of a conventional vortex. In fact, K is nonzero only on both sides of the $q = \pm 1$ domain walls as shown in Fig. 3(g). Zero mean value of K suggests that the whole pattern represented in Fig. 6 can move freely.

A. Synthetic examples

Below, we demonstrate the main kinds of moving collective states with the $q = \pm 1$ junctions. We discuss three solutions to Eqs. (A3) obtained on a 1024×1024 grid. In all cases, a high potential wall of radius $R \approx 250\xi$ ensures zero boundary conditions. The initial states have two domains placed at $x < 0$ and $x > 0$ and connected by domain walls $\psi_{\pm}^{(q)}(x)$ whose type q can be different depending on y . The driving amplitude f corresponds to Fig. 5 ($f^2/f_2^2 = 0.025$). The system dynamics is explicitly shown in the respective Supplemental Materials II, III, and IV that contain video presentations.

The first example has such initial state that $q = +1$ at $y \geq 0$ and $q = -1$ at $y < 0$. The solution shows that a HQV molecule rapidly appears at $\mathbf{r} = 0$, after which the whole picture becomes self-consistent and evolves steadily. As expected, the $q = \pm 1$ parts of the domain wall move in opposite directions and, since they are connected, rotate around $\mathbf{r} = 0$. A snapshot of $\phi_{\pm}(\mathbf{r})$ at some time moment is shown in Fig. 7. Clearly, rotation implies that linear velocity v grows with r . According to Fig. 5(b), multiple solutions with different v indeed coexist for the same set of boundary conditions. Since the range of v is limited, the uniformly rotating patterns cannot persist against arbitrarily increasing R ; it is remarkable, however, that they are still possible for $R = 250\xi$. The stability of the solution is related to the fact that its energy is less than the vacuum one. At the same time, a displacement of the HQV molecule from the center eventually makes the whole system lose its dynamical balance. Analogous patterns often form spontaneously

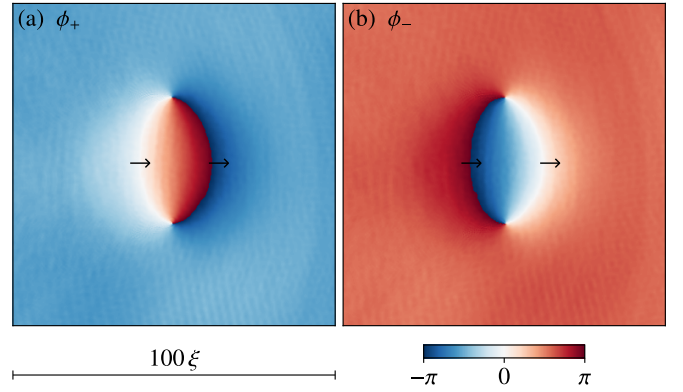


FIG. 8. A closed contour of two $q = \pm 1$ domain walls moving in space. (a) and (b) represent phases ϕ_{\pm} of two spin components. The arrows indicate the direction of motion. Parameters as in Fig. 7. The dynamics is shown in Supplemental Material III.

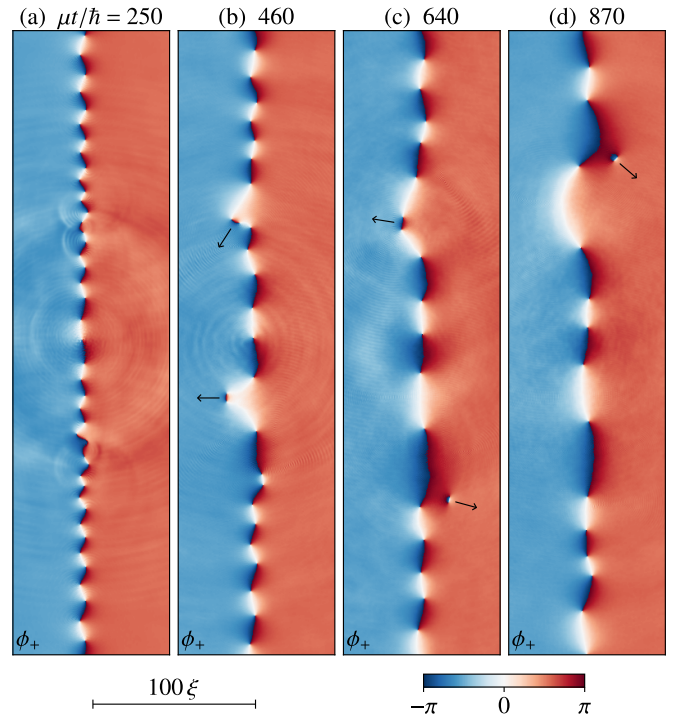


FIG. 9. Sequence of spatially alternating $q = \pm 1$ states formed after the breakup of the $q = 0$ domain wall. (a)–(d) correspond to different time moments. The arrows indicate the directions of motion of small composite solitons. The color map represents ϕ_+ . Parameters as in Fig. 7. The dynamics is shown in Supplemental Material IV.

in randomly prepared systems, yet, they usually have smaller sizes and lifetimes.

In the second example, the system evolves from the initial state with $q = +1$ at $|y| \leq a$ and $q = -1$ at $|y| > a$, where a is a relatively small distance equal to $12.5\xi = 0.05R$. The outer segments have the same q and rotate in opposite directions, so they eventually meet and cancel each other everywhere except the $|y| \leq a$ region in which the solution takes the form shown in Fig. 8. It is seen to be composed of two HQV molecules

and two $q = \pm 1$ domain walls that encapsulate some piece of one domain inside the other. In spite of opposite q , the average phase gradients of the domain walls have the same direction, because the respective pairs of their “left” and “right” domains are also mutually opposite. As a result, we have a composite soliton that moves as a unified object preserving its shape. Direct calculation shows that energy (2) is now greater than the vacuum energy. Thus, being stable in the dynamical sense, this pattern suffers the Landau damping and gradually decreases in size until two HQV molecules annihilate. Noteworthy, it moves in the direction of growing rather than decreasing phases, which corresponds to the bright-soliton section of Fig. 5(b).

The third solution evolves from the most simple initial state: $q = 0$ for each y . In the considered area of small f , such domain walls prove to be *dynamically* unstable, breaking up in a way similar to the snake (transverse) instability of the 2π domain walls in atomic BECs that is accompanied by formation of HQV molecules [23, 24]. However, in contrast to atomic BECs, the domain wall as such does not disappear but only reduces its symmetry by turning into a chain of the $q = \pm 1$ states connected by HQV molecules like in Fig. 6. The further evolution is illustrated in Fig. 9. With time, adjacent pairs of molecules annihilate or couple into composite solitons that detach from the wall and decay shortly, producing sound waves. As a result, the total energy of the system decreases.

B. Spontaneous phenomena

Up to now, we have focused on the solutions evolved from some special initial conditions obeying Eqs. (10)–(12). Bearing in mind optically driven microcavities, let us now consider a system with *zero* initial conditions that evolves owing to an arbitrarily slow increase in f . Initially—at very small f —all solutions are spin-symmetric ($\psi_+ = \psi_-$), so that the system is effectively one-component ($\psi_H \neq 0$, $\psi_V = 0$). However, as soon as f reaches its critical magnitude f_{thr} (B8), the driven mode is amplified sharply, which is accompanied by a rapid population of many new modes with nonzero wave vectors and “antisymmetric” spin states such that $\psi_+ = -\psi_-$ (accordingly, $\psi_H = 0$, $\psi_V \neq 0$). As a result, the spin symmetry breaks down and the system comes to a highly disordered state represented in Fig. 10(a).

Let us consider this process in more detail. The initial modulational instability, occurring at $f \gtrsim f_{\text{thr}}$ and $V\psi_H^2 \gtrsim 2\gamma$, involves a jump in ψ_H up to $V\psi_H^2 \approx 2D - \Omega$ that corresponds to the upper root of Eq. (B6). Such transition is, in essence, a sharp switch of a bistable system [49]. As a consequence, the spectra of elementary excitations (B7) take the form

$$\tilde{E}_H(k) = -i\gamma \pm \sqrt{E(k)[E(k) + \Omega]}, \quad (17)$$

$$\tilde{E}_V(k) = -i\gamma \pm \sqrt{E(k)[E(k) - \Omega]}, \quad (18)$$

where we assume that $D = \Omega$ for simplicity, $E(k) = \hbar^2 k^2 / 2m$ represents the bare dispersion law, and H, V indicate the polarization states. $\tilde{E}_H(k)$ is seen to have the Bogoliubov form, which means that ψ_H is indeed increased up to the point where

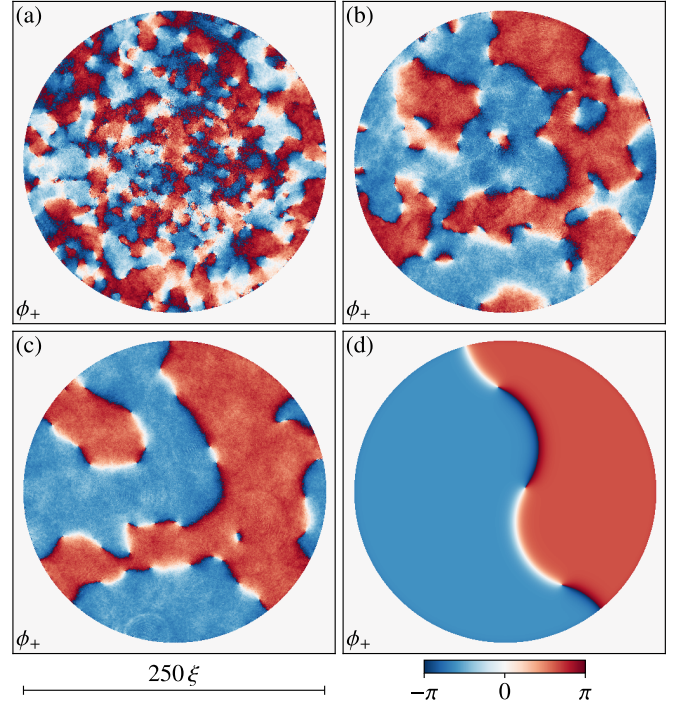


FIG. 10. Typical stages of evolution of a system with zero initial conditions under a very slow increase in f . (a) Highly disordered state soon after the spin symmetry breakdown. (b) Onset of phase domains. (c) Self-organization of nonstationary domains. (d) Eventual static solution at $f^2/f_2^2 \approx 0.14$. The color map represents ϕ_+ . Parameters: $D = \Omega$, $\gamma/\Omega = 5 \times 10^{-3}$, $R = 125 \xi$.

the respective instability is over ($\text{Im } \tilde{E}_H = -\gamma$). However, the same state shows a strong instability in ψ_V , owing to which the spin symmetry eventually breaks down. The characteristic time of this process \hbar/Γ is determined by $\Gamma = \max \text{Im } \tilde{E}_V(k) = \Omega/2 - \gamma$, thus, it is much shorter than the relaxation time \hbar/γ . The maximum of $\text{Im } \tilde{E}_V(k)$ is reached at $k = \sqrt{m\Omega}/\hbar$, which results in a significant spatial inhomogeneity. The respective scale k^{-1} is as small as $\sqrt{3}\xi$ for $D = \Omega$. Notice also that the individual phases of $\psi_V(\pm \mathbf{k})$ are not fixed in accordance with the Bogoliubov equation (B3), which implies the spontaneous character of the symmetry breaking.

Since the spin symmetry breaks down rapidly, the overall transition proceeds *nonglobally*: the signs of S_3 become unrelated already on the scale of several ξ . In this respect, the discussed process agrees with the Kibble-Zurek scenario for the nonadiabatic symmetry breaking in the early Universe [10] or superfluid liquids [11]. The analogy is substantiated by a direct connection between the characteristic time $2\hbar/\Omega$ and length scale $\hbar/\sqrt{m\Omega}$ of the transition. However, the spin symmetry breaking does not necessarily imply formation of phase domains, because $f_{\text{thr}} < f_1$ at small γ [see (B8), (B18)] and, thus, some interval of f has no stable vacuum states at all [50].

As soon as f reaches f_1 , a pair of new vacuum states with $\psi_+^* = \psi_-$ come into being. Since then, the evolution takes the form of self-organization. Large-scale domains start forming at its early stage [Fig. 10(b)], but the whole picture also contains a number of moving non-consolidated fragments simi-

lar to Fig. 8. In fact, even after the system has divided into domains [Fig. 10(c)], it still demonstrates motion of domain walls. A finite-sized system can occasionally stabilize completely [Fig. 10(d)]. According to our calculations, this occurs only when f becomes much larger than f_1 and the $q = \pm 1$ domain walls acquire a sufficiently high energy.

When f is increased further, the system exhibits dynamically stable domain walls with $q = 0$. Notice that even Fig. 3 suggests that the $q = 0$ states become less steep and, thus, less energetically costly than the $q = \pm 1$ ones as f increases. Figure 11 shows a crossover solution in which the two types of domain walls coexist. It evolved from zero initial conditions, similarly to Fig. 10, under increasing f^2 up to $\sim 0.16 f_2^2$. The $q = 0$ part of the domain wall is seen as a straight line segment characterized by opposite ϕ_+ and ϕ_- [Figs. 11(a) and 11(b)], high S_1 [Fig. 11(c)], and almost zero S_3 [Fig. 11(d)]. The rectilinear shape is indicative of the domain-wall tension that has an energetic origin in analogy to the 2π domain walls in atomic BECs [3, 7].

At smaller f , all $q = 0$ domain walls were confined inside HQV molecules much as in Fig. 6. The same kind of confined $q = 0$ states is represented in our last example by two tiny segments with $S_1 \approx +1$ whose end-point HQVs are visible in Fig. 11(d). In turn, the essentially large-scale $q = 0$ domain walls originate through the *deconfinement* of HQV pairs that is accompanied by a reordering and possible decay of HQVs upon increasing f . This process is, in a way, the opposite to the snake instability considered previously [Fig. 9(a)].

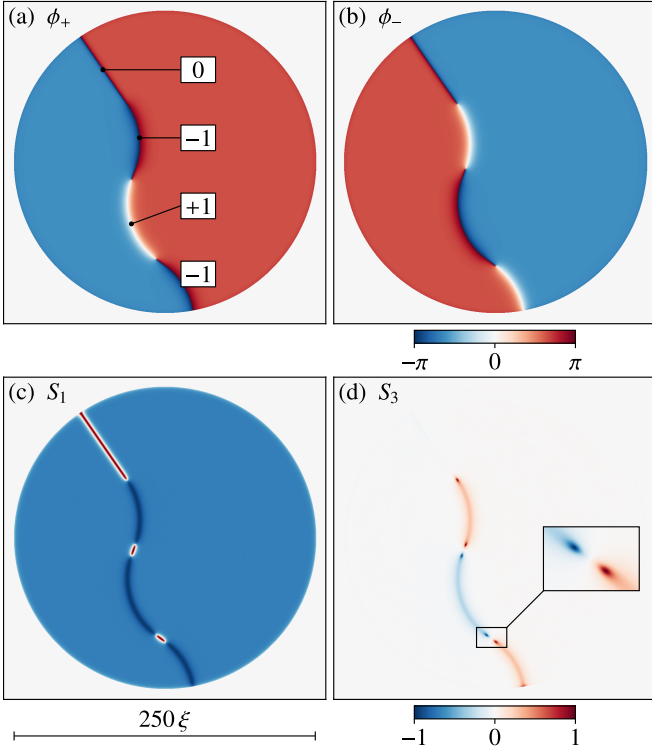


FIG. 11. Solution with coexisting $q = 0$ and $q = \pm 1$ domain walls. (a)–(d) represent ϕ_+ , ϕ_- , S_1 , S_3 . Numbers in (a) indicate q . Excitation intensity $f^2/f_2^2 \approx 0.16$, other parameters as in Fig. 10.

VI. CONCLUDING REMARKS

We have studied two kinds of phase domain walls formed in a coherently driven Bose system. One of them ($q = 0$) is found to be surprisingly analogous to domain walls typical of freely evolving BECs, whereas the other ($q = \pm 1$) is unconventional. The spin and spatiotemporal symmetries of the system break down spontaneously; a pair of its true vacuum states have opposite phases, neither of which is favored. Owing to the repulsive interaction and finite lifetime of quasiparticles, the system tends to reach either of these twin states at each point. Since, however, the rate of the symmetry-breaking transition is great even when f is increased slowly, its outcome is spatially dependent, similarly to the Kibble-Zurek scenario. The breakup of the trivial vacuum state is somewhat analogous to a spontaneously emergent polarization in *immiscible* two-component BECs [3, 9, 51, 52], although it does not rely upon the strong inter-component repulsion typical of such systems. Notice also that the spontaneous formation of domain walls was evidenced earlier in a three-component BEC in a magnetic field under the situation of a rapid phase transition [12].

Curiously, the special point $f = f_1$ in which the opposite-phase vacuum states come into being represents a sort of crossover between the driven and freely evolving BECs. The spectrum of elementary excitations at this point takes the Bogoliubov form and the $q = 0$ domain walls show a characteristic 2π jump of the relative phase. In general, the $q = 0$ domain walls acquire nonzero spin polarization depending on their state of motion (in a one-dimensional system) or give birth to HQV molecules through the transverse instability in two dimensions. Both of these phenomena also occur in atomic BECs [23, 24].

An important peculiarity of the system considered lies in the fact that its phase domains *per se* are asymptotically stable. Dynamical instability of the $q = 0$ domain walls does not end up in a globally uniform state as in [23, 24] but produces new domain walls with broken parity ($q = \pm 1$). Such solutions form a topological doublet whose components differ in the sign of the total phase variation across the wall. They tend to move in certain preferred directions and have fixed polarizations ($\text{sgn } S_3 = -q$), being in this respect similar to magnetic monopoles. In two dimensions, the $q = \pm 1$ domain walls naturally combine into collective states with long-range ordering, such as spontaneously rotating binary patterns or composite solitons containing multiple pairs of HQVs.

The obtained results hopefully allow to take a new view of a relation between atomic BECs and nonlinear optical systems. Our theoretical predictions can be directly verified based on the exciton-polariton fluids in state-of-the-art microcavities.

ACKNOWLEDGMENTS

I am grateful to N. N. Ipatov for stimulating discussions. The work was supported by the Foundation for the Advancement of Theoretical Physics and Mathematics “BASIS”.

Appendix A: Parameters of the polariton system

Optical field in a planar microcavity [13] has the shape of a standing wave whose transverse wave number $\pm k_z$ is fixed but the in-plane wave vector $\mathbf{k} = (k_x, k_y)$ remains free; $|\mathbf{k}|$ corresponds to the angle θ of incidence or emission of radiation relative to the z axis: $|\mathbf{k}/k_z| = \tan \theta$. In the range of small $|\mathbf{k}|$, the dispersion law of cavity photons takes a parabolic form

$$E_C(\mathbf{k}) = \frac{\hbar c}{\sqrt{\epsilon}} \sqrt{k_z^2 + \mathbf{k}^2} \approx E_0 + \frac{\hbar^2 \mathbf{k}^2}{2m_C}, \quad (\text{A1})$$

where ϵ is dielectric permittivity, E_0 is equal to $\hbar c|k_z|/\sqrt{\epsilon}$, and $m_C = \epsilon E_0/c^2$ is the photon mass. Energy E_0 can be tuned to resonance with quasi-two-dimensional excitons that form in a thin quantum well placed at the antinode of the electric field. Since the exciton mass greatly exceeds m_C , the exciton energy E_X is fairly independent of \mathbf{k} near $\mathbf{k} = 0$. The strong exciton-photon coupling, characterized by the Rabi energy \mathcal{R} , involves formation of polaritons. The polariton dispersion law

$$E_{\text{LP,UP}}(\mathbf{k}) = \frac{E_C(\mathbf{k}) + E_X}{2} \mp \frac{1}{2} \sqrt{(E_C(\mathbf{k}) - E_X)^2 + \mathcal{R}^2} \quad (\text{A2})$$

consists of the lower (LP) and upper (UP) polariton branches.

The external field is assumed to be a plane wave which has zero \mathbf{k} (so that its full wave vector is orthogonal to the cavity) and a frequency that slightly exceeds the respective resonance $E_{\text{LP}}(\mathbf{k} = 0)$. Since the excitation detuning D is noticeably less than \mathcal{R} , the upper polariton branch never gets populated, so we neglect it. Then the mean-field Eqs. (1) taking into account the correct form of $E_{\text{LP}}(\mathbf{k})$ are as follows:

$$i\hbar \frac{\partial \psi_{\pm}}{\partial t} = [-D + \hat{E}(-i\nabla) - i\gamma + V\psi_{\pm}^* \psi_{\pm}] \psi_{\pm} + \frac{\Omega}{2} \psi_{\mp} + f, \quad (\text{A3})$$

where operator function $\hat{E} = \hat{E}(-i\nabla)$ reproduces the dispersion law without the ground-state energy,

$$E(\mathbf{k}) = E_{\text{LP}}(\mathbf{k}) - E_{\text{LP}}(0). \quad (\text{A4})$$

Throughout this work, we employ Eqs. (A3) for accurate dynamical modeling, whereas basic features of domain walls are studied within the effective-mass approximation. In particular, we take $E_X = E_0$ when calculating $E_{\text{LP}}(\mathbf{k})$ in the former case and, self-consistently, $m = 2m_C$ in the second case when Eqs. (2), (3), or (10) are applied. The deviation between these models is not yet great for the chosen ratio $D/\mathcal{R} = 0.1$.

The set of parameters used in our numerical examples corresponds to a GaAs-based microcavity: $\epsilon = 12$, $E_0 = 1.5$ eV, $\mathcal{R} = 10$ meV, $D = \Omega = 1$ meV; γ is small and chosen arbitrarily. The only unconventional assumption is that Ω largely exceeds γ . Calculations show that phase domains spontaneously form in some range of f at $\Omega/\gamma \gtrsim 10$ (see also a discussion in [50]). However, in order to robustly observe both types of domain walls, one has to further increase Ω/γ up to $\sim 10^2$; for instance, Figs. 6, 10, and 11 are obtained at $\Omega/\gamma = 200$. In practice, high Ω/γ could originate from a structural anisotropy (e. g., owing to an in-plane mechanical stress [20] or magnetic field) combined with a high quality factor $Q \approx E_0/2\gamma$. These

conditions seem to be fairly achievable in the immediate future.

In modeling, any choice of $V > 0$ only fixes the units for f and ψ_{\pm} and does not affect the results. Physically, however, it is important that the mean-field theory holds true when Vn_{\pm} is as great as D and Ω . In accordance with Eq. (6) from [18], $V \approx \pi a_B C_X^2 e^2/\epsilon \approx 1.5 \times 10^{-14}$ eV cm², where $a_B \approx 8$ nm is the exciton Bohr radius and $C_X^2 = 1/2$ is the $k = 0$ exciton Hopfield factor for $E_X = E_0$. Consequently, in the state with $Vn_{\pm} = \mu = D + \Omega/2 = 1.5$ meV we have $n_{\pm} a_B^2 \approx 0.06$, so that the exciton gas is still dilute and the mean-field approximation is valid ([53]).

The interaction between same-spin excitons or polaritons is, in essence, Coulombic, so it is much stronger than the s -wave scattering of atoms in conventional BECs. On the other hand, the effective mass $m \sim 2\epsilon E_0/c^2$ is very small as compared even to free electrons. Accordingly, the healing length $\xi = \hbar/\sqrt{2mVn_{\pm}} = \hbar c/\sqrt{4\epsilon E_0 \mu} \approx 0.6 \mu\text{m}$ turns out to be close to the atomic one, but the respective sound velocity $v_s = \sqrt{\mu/m} = c\sqrt{\mu/2\epsilon E_0} \approx 0.0065 c$ is much greater. As a characteristic example, the disk-shaped pattern in Fig. 7 has the diameter of 0.3 mm and rotates with the period of 0.7 ns.

Appendix B: All vacuum states and elementary excitations

As a first step, one should find amplitudes $\bar{\psi}_{\pm}$ of stationary uniform solutions with $\mathbf{k} = 0$ (vacuum states). Provided that $\partial_t \psi_{\pm} = 0$ and $\nabla \psi_{\pm} = 0$, Eqs. (A3) take the form of two coupled algebraic equations

$$(-D - i\gamma + V\bar{\psi}_{\pm}^* \bar{\psi}_{\pm}) \bar{\psi}_{\pm} + \frac{\Omega}{2} \bar{\psi}_{\mp} + f = 0. \quad (\text{B1})$$

When a particular solution to (B1) for a given f is found, the respective spectrum of excitations can be calculated in a standard way based on the Bogoliubov equation. Namely, substitution of the ansatz

$$\psi_{\pm}(\mathbf{r}, t) = \bar{\psi}_{\pm} + \zeta_{\pm} e^{i(\mathbf{kr} - \tilde{E}t/\hbar)} + \eta_{\pm} e^{-i(\mathbf{kr} - \tilde{E}t/\hbar)} \quad (\text{B2})$$

with infinitesimal $|\zeta_{\pm}|$ and $|\eta_{\pm}|$ into (A3) leads one to a linear system

$$\left[\begin{pmatrix} A_+ & B_+ & \Omega/2 & 0 \\ -B_+^* & -A_+ & 0 & -\Omega/2 \\ \Omega/2 & 0 & A_- & B_- \\ 0 & -\Omega/2 & -B_-^* & -A_- \end{pmatrix} - (i\gamma + \tilde{E}) I_4 \right] \begin{pmatrix} \zeta_+ \\ \eta_+ \\ \zeta_- \\ \eta_- \end{pmatrix} = 0, \quad (\text{B3})$$

where

$$A_{\pm} = E(\mathbf{k}) - D + 2V|\bar{\psi}_{\pm}|^2, \quad B_{\pm} = V\bar{\psi}_{\pm}^2, \quad (\text{B4})$$

and I_4 is the 4×4 identity matrix. Solving the equation $\det[\cdot] = 0$ yields the sought-for dispersion law $\tilde{E}_i = \tilde{E}_i(\mathbf{k})$ that has four branches ($i = 1, 2, 3, 4$). Stability of the underlying vacuum states is determined by quantity

$$\Gamma = \max_{\mathbf{k}, i} \text{Im } \tilde{E}_i(\mathbf{k}). \quad (\text{B5})$$

If $\Gamma < 0$, the solution $\tilde{\psi}_\pm$ to Eqs. (B1) is *asymptotically stable* (attractive), because any small deviation from it decays with time. And vice versa, all solutions with $\Gamma > 0$ are destroyed by arbitrarily small fluctuations and should thus be considered as false vacuum states.

In general, Eqs. (B1) have up to nine solutions for each f , six of which can be stable. They fall into three classes. The first is one or two spin-symmetric solutions such that $\tilde{\psi}_+ = \tilde{\psi}_-$; the second is a doublet of states with opposite spin polarizations, $|\tilde{\psi}_+| \neq |\tilde{\psi}_-|$; the third is a doublet with $\tilde{\psi}_\pm^* = \tilde{\psi}_\mp$ at $\gamma \rightarrow 0$ that consists of two solutions with opposite *phases*. The last pair turns out to be the sole kind of stable vacuum states in a finite range of f . In order to prove this statement conclusively, we should consider all classes of solutions and analyze their stability.

1. The *spin-symmetric states* ($\tilde{\psi}_+ = \tilde{\psi}_-$) exist for each f and are the only solutions at $f \rightarrow 0$ as well as $f \rightarrow \infty$. Taking the absolute square of (B1) readily leads one to

$$f^2 = \frac{u}{2V} \left[\left(D - \frac{\Omega}{2} - \frac{u}{2} \right)^2 + \gamma^2 \right], \quad (\text{B6})$$

where $u = Vn = 2V|\tilde{\psi}_\pm|^2$ corresponds to the density of the full number of particles. The spectrum of excitations is

$$\tilde{E}(\mathbf{k}) = -i\gamma \pm \frac{1}{2} \sqrt{[2(D - E(\mathbf{k}) - u) \pm \Omega]^2 - u^2}. \quad (\text{B7})$$

At $u \rightarrow 0$ and $f \rightarrow 0$, we have $\Gamma = -\gamma$. Upon increasing f and u , quantity Γ changes its sign in the critical point $u = 2\gamma$ where the system undergoes modulational instability. Specifically, $\text{Im } \tilde{E}(\mathbf{k})$ reaches zero on the circle $|\mathbf{k}| = k_*$ such that $E(k_*) = D - \Omega/2 - 2\gamma$. (By definition, $E(k) \geq 0$, so we suppose that $D - \Omega/2 > 2\gamma$.) The respective threshold value of f^2 is

$$f_{\text{thr}}^2 = \frac{\gamma}{V} \left[\left(D - \frac{\Omega}{2} - \gamma \right)^2 + \gamma^2 \right]. \quad (\text{B8})$$

Once this threshold is reached, u starts growing spontaneously (even if f is kept constant) up to the magnitude $u \gtrsim 2D - \Omega$ that corresponds the alternative root of (B6) for the same f . Such a switch between two vacuum states, mediated by *transient* excitation of many modes with $\mathbf{k} \neq 0$, was studied earlier in the case of a scalar bistable system [49]. The two-component system with $D \sim \Omega \gg \gamma$ behaves differently in that its upper stationary solution obeying (B6) is unstable with respect to the spin symmetry breaking. Technically, one can make sure that the eigenstates ζ_\pm and η_\pm corresponding to $\text{Im } \tilde{E} > 0$ are anti-symmetric ($\zeta_+ = -\zeta_-$, $\eta_+ = -\eta_-$), so their spontaneous amplification necessarily breaks the spin symmetry (see Sec. V B).

The second $\Gamma = 0$ point in which the spin-symmetric states become stable again is reached at $Vf^2 \approx \Omega^2(D + \Omega/2)$. Notice that the ratio between this value and Vf_{thr}^2 occurs to be indefinitely great at $\gamma \rightarrow 0$.

2. The *asymmetric solutions* with $\tilde{\psi}_+ \neq \tilde{\psi}_-$ exist in a finite area of u and f . Taking the difference of Eqs. (B1), separating the terms proportional to $\tilde{\psi}_\pm$, and proceeding to their absolute squares allow one to see that

$$u_+ u_- = (\mu - u)^2 + \gamma^2 \quad \text{if } u_+ \neq u_-, \quad (\text{B9})$$

where $u_\pm = Vn_\pm = V|\tilde{\psi}_\pm|^2$, $u = Vn = u_+ + u_-$, and $\mu = D + \Omega/2$. The inequality $(u_+ - u_-)^2 > 0$ together with (B9) is equivalent to $l_1 < u < l_2$, where

$$l_{1,2} = \frac{2}{3} (2\mu \mp \sqrt{\mu^2 - 3\gamma^2}). \quad (\text{B10})$$

Employing (B9) allows one to derive the solutions to (B1) in a parametric form. Specifically, f^2 as well as $\tilde{\psi}_\pm$ can be found as functions of only one real variable, u , defined on the interval (l_1, l_2) . Function $f^2(u)$ is single-valued and has the form

$$Vf^2 = (2\mu - u)(D - u)^2 + \frac{\gamma^2(2D - u)^2}{2\mu - u}. \quad (\text{B11})$$

For each u , there is a doublet of solutions which transform into each other by exchanging $\tilde{\psi}_+$ and $\tilde{\psi}_-$: $\tilde{\psi}_{\pm(\mp)} = \sqrt{u_{1,2}/V} e^{i\alpha_{1,2}}$, where $u_{1,2}$ and $e^{i\alpha_{1,2}}$ are determined unambiguously,

$$u_{1,2} = \frac{u}{2} \pm \frac{1}{2} \sqrt{u^2 - 4[(\mu - u)^2 + \gamma^2]}, \quad (\text{B12})$$

$$\alpha_2 - \alpha_1 = \arccos \left[\frac{1}{\sqrt{(\mu - u)^2 + \gamma^2}} \left(\mu - u + \frac{2\gamma^2}{2\mu - u} \right) \right], \quad (\text{B13})$$

$$e^{i\alpha_{1,2}} = \frac{\sqrt{Vf^2}}{(D + i\gamma - u_{1,2}) \sqrt{u_{1,2}} - (\Omega/2) \sqrt{u_{2,1}} e^{i(\alpha_{2,1} - \alpha_{1,2})}}. \quad (\text{B14})$$

Notice that $u_2 < u_1$ and $0 < \alpha_2 - \alpha_1 < \pi$. The right-hand side of (B14) is expressed through (B11)–(B13) those, in turn, depend solely on u . The radicand in (B12) is positive and the argument of arc cosine in (B13) lies in the interval $(-1, 1)$ as long as $u \in (l_1, l_2)$.

The spectrum of excitations is also parameterized by u and has the following form,

$$\begin{aligned} \tilde{E}(\mathbf{k}) = & -i\gamma \pm \frac{1}{\sqrt{2}} \left\{ 2(E(\mathbf{k}) - D + u)^2 + u^2 - 6(\mu - u)^2 + \frac{g^2}{2} - 6\gamma^2 \right. \\ & \pm \left[(u^2 - 4(\mu - u)^2 - 4\gamma^2)(4E(\mathbf{k}) - 4D + 3u)^2 \right. \\ & \quad \left. + 4g^2(E(\mathbf{k}) - D + u)^2 - g^2u^2 \right. \\ & \quad \left. \left. + 4g^2 \left(\mu - u + \frac{2\gamma^2}{2\mu - u} \right)^2 \right]^{1/2} \right\}^{1/2}. \quad (\text{B15}) \end{aligned}$$

Expressions (B11)–(B15) constitute an *exact* representation of all asymmetric vacuum states in a system with arbitrary D , Ω , and γ .

If $D \sim \Omega \gg \gamma$, quartic equation $df/du = 0$ has four real-valued roots, of which two, $r_{1,2}$, fall within (l_1, l_2) . Let $r_1 < r_2$, then the first relevant interval $l_1 < u < r_1$ has a positive slope ($du/df > 0$) and contains the *spin* doublets whose stability (sign of Γ) depends on f . The next one, $r_1 < u < r_2$, is wholly unstable ($du/df < 0$ and $\Gamma > 0$). The last interval $r_2 < u < l_2$ contains the *opposite-phase* doublets which, by contrast, are stable for each f . At $u \rightarrow l_2$, both $u_+ - u_-$ and $\alpha_+ - \alpha_-$ tend to zero, (B11) coincides with (B6), and (B15) coincides with (B7); moreover, exactly at this point the spin-symmetric solutions become stable again, displaying the transcritical bifurcation.

2-a. The *spin* doublets have a moderate amplitude such that $D < u \sim \mu$, therefore, the last term in (B11) can be neglected in the limit $\gamma \rightarrow 0$. This branch of solutions was extensively studied in Ref. [50] where Eq. (B11) was first derived. Here, we only notice that the spin doublets are unstable at small f , in contrast to the spin-symmetric states. The instability does not necessarily imply scattering into the $\mathbf{k} \neq 0$ modes. For instance, at $D = \Omega$, $\gamma \rightarrow 0$, and $\mathbf{k} = 0$, the energy of excitations (B15) becomes

$$\tilde{E}(0) = -i\gamma \pm \frac{1}{\sqrt{2}} \left\{ (u - \Omega)(-3u + 11\Omega) \pm |u - \Omega|(-27u^2 + 126\Omega u - 131\Omega^2)^{1/2} \right\}^{1/2}. \quad (\text{B16})$$

The inner radicand is negative, resulting in $\Gamma > 0$, for each u up to $u \approx 1.56\Omega = 1.04\mu$ and, accordingly, $f^2(u) \approx 0.3f^2(l_2)$. The two modes which get amplified at this critical point in the course of decreasing f are split in energy, which corresponds to the Hopf bifurcation.

2-b. The *phase* doublets are of prime importance in our current study. Below, we show them to exist and be stable even at $f \rightarrow 0$ if $\gamma \rightarrow 0$. Based on Eqs. (B12) and (B13), we find their spin polarizations and phases as explicit functions of the driving field. We identify the exceptional points in which the spectrum of excitations takes the Bogoliubov form typical of superfluid liquids and atomic BECs. Normally, the spectrum has a gap that is also calculated explicitly.

Unlike Ref. [50], we have to take into account the last term of (B11) that plays a major role in spite of small γ . Indeed, in accordance with (B10), l_2 tends to $2\mu - \gamma^2/\mu$ at $\gamma \rightarrow 0$, thus, that last term remains finite at $u \rightarrow l_2$, whereas the first term vanishes.

The top branch of solutions begins at $u = r_2$ that is the upper root of $df/du = 0$ lying within (l_1, l_2) . After substituting $u = 2\mu - \rho$, this equation takes the form

$$3\rho^4 - 4\rho^3(D + \Omega) + \rho^2[(D + \Omega)^2 + \gamma^2] - \gamma^2\Omega^2 = 0, \quad (\text{B17})$$

and we seek the minimum positive ρ satisfying it. Clearly, at small γ this is $\rho \approx \gamma\Omega/(D + \Omega)$. The respective value of $f^2(u)$,

$$f_1^2 = \frac{2\gamma\Omega}{V}(D + \Omega), \quad (\text{B18})$$

represents the critical intensity of the driving field. The second limiting point is simply $f^2(l_2)$, which evaluates to

$$f_2^2 = \frac{\Omega^2}{V} \left(D + \frac{\Omega}{2} \right). \quad (\text{B19})$$

It is seen that $f_2 \gg f_1$ at $\gamma \rightarrow 0$, however, the overall change in u throughout the top branch is very small ($\sim \gamma$). Strictly speaking, (B11) is senseless at $\gamma = 0$ because of the 0/0 indeterminacy in its last term, which means that u becomes independent of f . However, everything remains regular at $\gamma \rightarrow 0^+$. Below, we always suppose that $D \sim \Omega \gg \gamma$, thus, we can substitute $u = 2\mu - \rho$ directly into (B11) and then drop the ρ^4 and ρ^3 terms, which eventually yields

$$u = 2\mu - \frac{Vf^2}{2(D + \Omega)^2} \left(1 - \sqrt{1 - \frac{f_1^4}{f^4}} \right) \quad (\text{B20})$$

(the second root would match the unstable branch of solutions with $du/df < 0$). In the case when $f^4 \gg f_1^4$, this result can be simplified further to yield

$$u = 2\mu - \frac{\gamma^2\Omega^2}{Vf^2}. \quad (\text{B21})$$

Substituting (B21) into (B12) and (B13) allows one to find the spin polarization S_3 and phases at high f along the top branch. In particular,

$$S_3 = \pm \frac{\gamma}{\mu} \sqrt{\frac{f_2^2}{f^2} - 1}. \quad (\text{B22})$$

It turns out that u_+ and u_- are very close almost irrespective of f : even the maximum $|S_3|$ reached at $f = f_1$ is of the order of $\sqrt{\gamma/\mu}$. On the other hand, it is clear from (B14) that condition $u_+ = u_-$ necessarily implies $e^{i\alpha_+} = e^{-i\alpha_-}$ as long as $\gamma \rightarrow 0$. As a result, from (B13) and (B14) we have

$$\alpha_{\pm(\mp)} = \pm \arccos \left(-\frac{f}{f_2} \right). \quad (\text{B23})$$

for two solutions in the phase doublet (generally, the sign of $\sin(\alpha_- - \alpha_+)$ is equal to the sign of S_3). The fact that both components are π -shifted relative to the driving field at $f = f_2$ agrees with the spin-symmetric model in the range of great f and u .

Proceeding to the problem of excitations, notice that everything in (B15) hardly depends on f except the last (fractional) term that can be rewritten as

$$\frac{\gamma^2}{2\mu - u} = \frac{Vf^2}{\Omega^2} = \frac{\mu f^2}{f_2^2} \quad (\text{B24})$$

in accordance with (B21) and (B19). We substitute (B24) into (B15) and assume that $u = 2\mu$ in all regular terms, which leads us to the following explicit form of the spectrum,

$$\tilde{E}(\mathbf{k}) = -i\gamma \pm \left\{ (E(\mathbf{k}) + D + \Omega)^2 - D(D + \Omega) \pm \Omega \left[(E(\mathbf{k}) + D + \Omega)^2 - 4\mu^2 \left(\frac{f^2}{f_2^2} - \frac{f^4}{f_2^4} \right) \right]^{1/2} \right\}^{1/2}. \quad (\text{B25})$$

It is seen that $\Gamma = -\gamma$ for each f , i.e., all phase doublets are stable, which is intimately connected to the fact that the spectrum has a gap $E_g = \min_{\mathbf{k},i} |\text{Re } \tilde{E}_i(\mathbf{k})|$. The minimum over \mathbf{k} is reached at $\mathbf{k} = 0$, so the gap width evaluates to

$$E_g = \sqrt{\Omega} \left\{ D + \Omega - \left[(D + \Omega)^2 - 4\mu^2 \left(\frac{f^2}{f_2^2} - \frac{f^4}{f_2^4} \right) \right]^{1/2} \right\}^{1/2}. \quad (\text{B26})$$

Clearly, E_g tends to zero at $f = f_1 \propto \sqrt{\gamma} \rightarrow 0$ as well as $f = f_2$. In both of these points, the gapless branches of (B25) take the Bogoliubov form

$$\tilde{E}(\mathbf{k}) = -i\gamma \pm \sqrt{E(\mathbf{k})[E(\mathbf{k}) + 2\mu]}. \quad (\text{B27})$$

Thus, $\mu \equiv D + \Omega/2$ matches the chemical potential of an equilibrium BEC.

-
- [1] A. J. Leggett, Bose-Einstein condensation in the alkali gases: Some fundamental concepts, *Rev. Mod. Phys.* **73**, 307 (2001).
 - [2] Y. Tanaka, Multicomponent superconductivity based on multi-band superconductors, *Supercond. Sci. Technol.* **28**, 034002 (2015).
 - [3] D. T. Son and M. A. Stephanov, Domain walls of relative phase in two-component Bose-Einstein condensates, *Phys. Rev. A* **65**, 063621 (2002).
 - [4] Y. Tanaka, Soliton in Two-Band Superconductor, *Phys. Rev. Lett.* **88**, 017002 (2001).
 - [5] M. Eto, K. Kasamatsu, M. Nitta, H. Takeuchi, and M. Tsubota, Interaction of half-quantized vortices in two-component Bose-Einstein condensates, *Phys. Rev. A* **83**, 063603 (2011).
 - [6] M. Tylutki, L. P. Pitaevskii, A. Recati, and S. Stringari, Confinement and precession of vortex pairs in coherently coupled Bose-Einstein condensates, *Phys. Rev. A* **93**, 043623 (2016).
 - [7] M. Eto and M. Nitta, Confinement of half-quantized vortices in coherently coupled Bose-Einstein condensates: Simulating quark confinement in a QCD-like theory, *Phys. Rev. A* **97**, 023613 (2018).
 - [8] M. Eto, K. Ikeno, and M. Nitta, Collision dynamics and reactions of fractional vortex molecules in coherently coupled Bose-Einstein condensates, *Phys. Rev. Res.* **2**, 033373 (2020).
 - [9] A. Recati and S. Stringari, Coherently Coupled Mixtures of Ultracold Atomic Gases, *Annu. Rev. Condens. Matter Phys.* **13**, 407 (2022).
 - [10] T. W. B. Kibble, Some implications of a cosmological phase transition, *Phys. Rep.* **67**, 183 (1980).
 - [11] W. H. Zurek, Cosmological experiments in superfluid helium?, *Nature* **317**, 505 (1985).
 - [12] S. Kang, S. W. Seo, H. Takeuchi, and Y. Shin, Observation of Wall-Vortex Composite Defects in a Spinor Bose-Einstein Condensate, *Phys. Rev. Lett.* **122**, 095301 (2019).
 - [13] A. V. Kavokin, J. J. Baumberg, G. Malpuech, and P. Laussy, *Microcavities*, 2nd ed. (Oxford University Press, New York, 2017).
 - [14] S. S. Gavrilov, Nonequilibrium transitions, chaos, and chimera states in exciton-polariton systems, *Phys. Usp.* **63**, 123 (2020).
 - [15] J. Kasprzak, M. Richard, S. Kundermann, A. Baas, P. Jeambrun, J. M. J. Keeling, F. M. Marchetti, M. H. Szymańska, R. André, J. L. Staehli, V. Savona, P. B. Littlewood, B. Deveaud, and L. S. Dang, Bose-Einstein condensation of exciton polaritons, *Nature* **443**, 409 (2006).
 - [16] A. Baas, J.-P. Karr, M. Romanelli, A. Bramati, and E. Giacobino, Quantum Degeneracy of Microcavity Polaritons, *Phys. Rev. Lett.* **96**, 176401 (2006).
 - [17] C. Ciuti, V. Savona, C. Piermarocchi, A. Quattropani, and P. Schwendimann, Role of the exchange of carriers in elastic exciton-exciton scattering in quantum wells, *Phys. Rev. B* **58**, 7926 (1998).
 - [18] M. Vladimirova, S. Cronenberger, D. Scalbert, K. V. Kavokin, A. Miard, A. Lemaître, J. Bloch, D. Solnyshkov, G. Malpuech, and A. V. Kavokin, Polariton-polariton interaction constants in microcavities, *Phys. Rev. B* **82**, 075301 (2010).
 - [19] A. V. Sekretenko, S. S. Gavrilov, and V. D. Kulakovskii, Polariton-polariton interactions in microcavities under a resonant 10 to 100 picosecond pulse excitation, *Phys. Rev. B* **88**, 195302 (2013).
 - [20] S. S. Gavrilov, A. S. Brichkin, S. I. Novikov, S. Höfling, C. Schneider, M. Kamp, A. Forchel, and V. D. Kulakovskii, Nonlinear route to intrinsic Josephson oscillations in spinor cavity-polariton condensates, *Phys. Rev. B* **90**, 235309 (2014).
 - [21] S. Pigeon, I. Carusotto, and C. Ciuti, Hydrodynamic nucleation of vortices and solitons in a resonantly excited polariton superfluid, *Phys. Rev. B* **83**, 144513 (2011).
 - [22] S. S. Gavrilov, Spontaneous formation of vortices and gray solitons in a spinor polariton fluid under coherent driving, *Phys. Rev. B* **102**, 104307 (2020).
 - [23] K. Ihara and K. Kasamatsu, Transverse instability and disintegration of a domain wall of a relative phase in coherently coupled two-component Bose-Einstein condensates, *Phys. Rev. A* **100**, 013630 (2019).
 - [24] A. Gallemí, L. P. Pitaevskii, S. Stringari, and A. Recati, Decay of the relative phase domain wall into confined vortex pairs: The case of a coherently coupled bosonic mixture, *Phys. Rev. A* **100**, 023607 (2019).
 - [25] A. Gallemí, M. Guilleumas, R. Mayol, and A. M. Mateo, Multidimensional Josephson vortices in spin-orbit-coupled Bose-Einstein condensates: Snake instability and decay through vortex dipoles, *Phys. Rev. A* **93**, 033618 (2016).
 - [26] C. Qu, M. Tylutki, S. Stringari, and L. P. Pitaevskii, Magnetic solitons in Rabi-coupled Bose-Einstein condensates, *Phys. Rev. A* **95**, 033614 (2017).
 - [27] X. Yu and P. B. Blakie, Dark-soliton-like magnetic domain walls in a two-dimensional ferromagnetic superfluid, *Phys. Rev. Res.* **3**, 023043 (2021).
 - [28] X. Yu and P. B. Blakie, Propagating Ferrodark Solitons in a Superfluid: Exact Solutions and Anomalous Dynamics, *Phys. Rev. Lett.* **128**, 125301 (2022).
 - [29] L. Pitaevskii and S. Stringari, *Bose-Einstein Condensation and Superfluidity* (Oxford University Press, New York, 2016).
 - [30] S. S. Gavrilov, Nonequilibrium transitions, chaos, and chimera states in exciton-polariton systems, *Usp. Fiz. Nauk* **190**, 137 (2020).
 - [31] V. Rubakov, *Classical Theory of Gauge Fields* (Princeton University Press, 2002).
 - [32] T. Boulier, H. Terças, D. D. Solnyshkov, Q. Glorieux, E. Giacobino, G. Malpuech, and A. Bramati, Vortex Chain in a Resonantly Pumped Polariton Superfluid, *Sci. Rep.* **5**, 9230 (2015).
 - [33] L. Dominici, G. Dagvadorj, J. M. Fellows, D. Ballarini, M. De Giorgi, F. M. Marchetti, B. Piccirillo, L. Marrucci, A. Bramati, G. Gigli, M. H. Szymańska, and D. Sanvitto, Vortex and half-vortex dynamics in a nonlinear spinor quantum fluid, *Sci. Adv.* **1**, e1500807 (2015).
 - [34] L. Dominici, R. Carretero-González, A. Gianfrate, J. Cuevas-Maraver, A. S. Rodrigues, D. J. Frantzeskakis, G. Lerario, D. Ballarini, M. De Giorgi, G. Gigli, P. G. Kevrekidis, and D. Sanvitto, Interactions and scattering of quantum vortices in a polariton fluid, *Nat. Commun.* **9**, 1467 (2018).
 - [35] I. Carusotto and C. Ciuti, Quantum fluids of light, *Rev. Mod. Phys.* **85**, 299 (2013).
 - [36] A. Amo, S. Pigeon, D. Sanvitto, V. G. Sala, R. Hivet, I. Carusotto, F. Pisanello, G. Leménager, R. Houdré, E. Giacobino, C. Ciuti, and A. Bramati, Polariton Superfluids Reveal Quantum Hydrodynamic Solitons, *Science* **332**, 1167 (2011).
 - [37] S. Pigeon and A. Bramati, Sustained propagation and control of topological excitations in polariton superfluid, *New J. Phys.* **19**, 095004 (2017).
 - [38] D. M. Whittaker, Vortices in the microcavity optical parametric oscillator, *Superlattices Microstruct.* **41**, 297 (2007).
 - [39] D. N. Krizhanovskii, D. M. Whittaker, R. A. Bradley, K. Guda, D. Sarkar, D. Sanvitto, L. Viña, E. Cerda, P. Santos, K. Biermann, R. Hey, and M. S. Skolnick, Effect of Interactions on

- Vortices in a Nonequilibrium Polariton Condensate, *Phys. Rev. Lett.* **104**, 126402 (2010).
- [40] F. M. Marchetti, M. H. Szymańska, C. Tejedor, and D. M. Whittaker, Spontaneous and Triggered Vortices in Polariton Optical-Parametric-Oscillator Superfluids, *Phys. Rev. Lett.* **105**, 063902 (2010).
- [41] D. Sanvitto, F. M. Marchetti, M. H. Szymańska, G. Tosi, M. Baudisch, F. P. Laussy, D. N. Krizhanovskii, M. S. Skolnick, L. Marrucci, A. Lemaître, J. Bloch, C. Tejedor, and L. Viña, Persistent currents and quantized vortices in a polariton superfluid, *Nat. Phys.* **6**, 527 (2010).
- [42] G. Dagvadorj, J. M. Fellows, S. Matyjaśkiewicz, F. M. Marchetti, I. Carusotto, and M. H. Szymańska, Nonequilibrium Phase Transition in a Two-Dimensional Driven Open Quantum System, *Phys. Rev. X* **5**, 041028 (2015).
- [43] S. V. Koniakhin, O. Bleu, D. D. Stupin, S. Pigeon, A. Maitre, F. Claude, G. Lerario, Q. Glorieux, A. Bramati, D. Solnyshkov, and G. Malpuech, Stationary Quantum Vortex Street in a Driven-Dissipative Quantum Fluid of Light, *Phys. Rev. Lett.* **123**, 215301 (2019).
- [44] F. Claude, S. V. Koniakhin, A. Maître, S. Pigeon, G. Lerario, D. D. Stupin, Q. Glorieux, E. Giacobino, D. Solnyshkov, G. Malpuech, and A. Bramati, Taming the snake instabilities in a polariton superfluid, *Optica* **7**, 1660 (2020).
- [45] J. Kierzenka and L. F. Shampine, A BVP solver based on residual control and the Matlab PSE, *ACM Trans. Math. Softw.* **27**, 299 (2001).
- [46] P. Virtanen, R. Gommers, T. E. Oliphant, M. Haberland, T. Reddy, D. Cournapeau, E. Burovski, P. Peterson, W. Weckesser, J. Bright, S. J. van der Walt, M. Brett, J. Wilson, K. J. Millman, N. Mayorov, A. R. J. Nelson, E. Jones, R. Kern, E. Larson, C. J. Carey, Í. Polat, Y. Feng, E. W. Moore, J. VanderPlas, D. Laxalde, J. Perktold, R. Cimrman, I. Henriksen, E. A. Quintero, C. R. Harris, A. M. Archibald, A. H. Ribeiro, F. Pedregosa, P. van Mulbregt, and SciPy 1.0 Contributors, SciPy 1.0: Fundamental Algorithms for Scientific Computing in Python, *Nat. Methods* **17**, 261 (2020).
- [47] A. M. Kamchatnov and L. P. Pitaevskii, Stabilization of Solitons Generated by a Supersonic Flow of Bose-Einstein Condensate Past an Obstacle, *Phys. Rev. Lett.* **100**, 160402 (2008).
- [48] J. R. Dormand and P. J. Prince, A family of embedded Runge-Kutta formulae, *J. Comput. Appl. Math.* **6**, 19 (1980).
- [49] S. S. Gavrilov, Blowup dynamics of coherently driven polariton condensates, *Phys. Rev. B* **90**, 205303 (2014).
- [50] S. S. Gavrilov, Spin oscillations of a single-mode polariton system driven by a plane wave, *Phys. Rev. B* **106**, 045304 (2022).
- [51] T. Zibold, E. Nicklas, C. Gross, and M. K. Oberthaler, Classical Bifurcation at the Transition from Rabi to Josephson Dynamics, *Phys. Rev. Lett.* **105**, 204101 (2010).
- [52] R. Cominotti, A. Berti, C. Dulin, C. Rogora, G. Lamporesi, I. Carusotto, A. Recati, A. Zenesini, and G. Ferrari, Ferromagnetism in an Extended Coherently Coupled Atomic Superfluid, *Phys. Rev. X* **13**, 021037 (2023).
- [53] L. V. Keldysh, Coherent states of excitons, *Phys. Usp.* **60**, 1180 (2017).